Improvements of the Moreau–Jean time integration scheme for multi-body systems with clearances and large rotations

Vincent Acary

Sixth Symposium of the European Network for Nonsmooth Dynamics (ENNSD)
September 6-7, 2017, Eindhoven University of Technology, The Netherlands.

joint work N. Akhadkar and B. Brogliato

Motivations

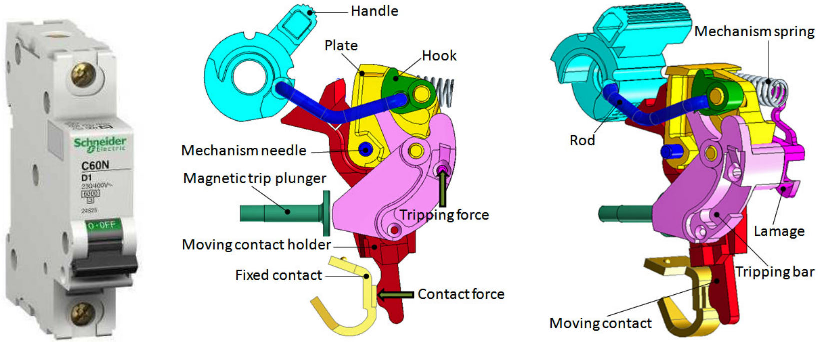

(a) External view (b) View-1. (c) View-2.

Figure: Schneider Electric C-60 circuit breaker mechanism.

Motivations

Main motivations

- Analysis of the influence of the manufacturing tolerances on the functional conditions of mechanisms.
- Monte-Carlo simulations to analyze the sensitivity

Means/Requirements

- Accurate modeling of rigid body dynamics with large rotations
- Modeling of clearances as frictional contact interfaces with gaps and restitution
- Avoid violation of constraints or penetrations if clearances are tight
- Efficient and robust numerical simulations to perform sensitivity analysis

Frictional contact interfaces

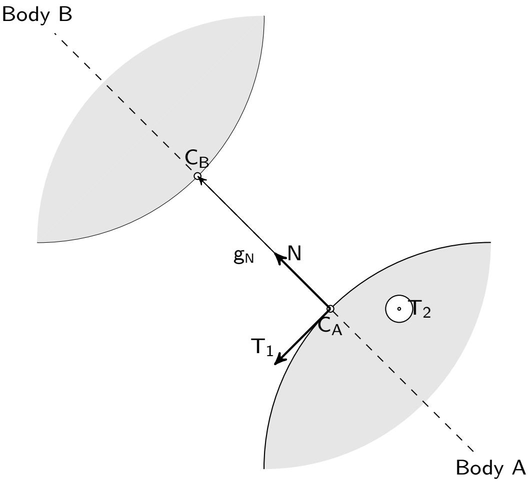

Figure: Contact local frame.

Frictional contact interfaces

Signorini contact law at the position level

$$0 \leqslant g_{\mathrm{N}} \perp r_{\mathrm{N}} \geqslant 0. \tag{1}$$

Signorini contact law at the velocity level $u_{\mathrm{N}} = \dot{g}_{\mathrm{N}}$

$$0 \leqslant u_{\mathrm{N}} \perp r_{\mathrm{N}} \geqslant 0, \quad \text{if} \quad g_{\mathrm{N}} = 0. \tag{2}$$

Newton impact law contact

$$u_{\mathrm{N}}^{+} = -e_r u_{\mathrm{N}}^{-}, \text{ if } g_{\mathrm{N}} = 0 \text{ and } u_{\mathrm{N}}^{-} \leqslant 0, \tag{3}$$

e_r coefficient of restitution

Frictional contact interfaces

Coulomb friction law

$$r \in K = \{r \in \mathbb{R}^3, ||r_{\mathrm{T}}|| \leqslant \mu r_{\mathrm{N}}\}. \tag{4}$$

$$\begin{cases} r = 0 & \text{if } g_{\mathrm{N}} > 0 \quad \text{(no contact)} \\ r = 0, u_{\mathrm{N}} \geqslant 0 & \text{if } g_{\mathrm{N}} = 0 \quad \text{(take-off)} \\ r \in K, u = 0 & \text{if } g_{\mathrm{N}} = 0 \quad \text{(sticking)} \\ r \in \partial K, u_{\mathrm{N}} = 0, \exists\, \beta > 0, u_{\mathrm{T}} = -\beta r_{\mathrm{T}} & \text{if } g_{\mathrm{N}} = 0 \quad \text{(sliding)} \end{cases} \tag{5}$$

Coulomb friction law as a second order cone complementarity

$$K^* \ni \widehat{u} \perp r \in K. \tag{6}$$

with the modified relative velocity $\widehat{u} := u + \mu ||u_{\mathrm{T}}|| \mathrm{N}$ and the dual cone of K, *i.e.*,

$$K^* = \{z \in \boldsymbol{R}^3 \mid z^T x \geqslant 0 \text{ for all } x \in K\}$$

Frictional contact interfaces

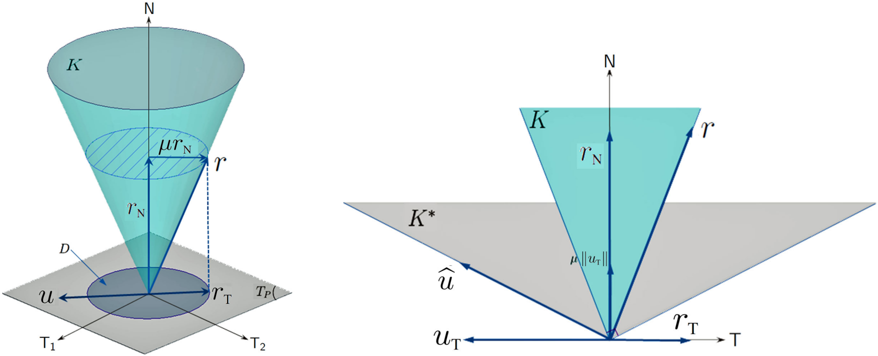

(a) 3D Coulomb's friction cone, the sliding case.

(b) Sliding case with modified velocity $\widehat{u}$, $r \in \partial K$.

Figure: Coulomb's Friction law.

Newton-Euler formulation of the equation of motion

Coordinates

- $x_{\rm g} \in \boldsymbol{R}^3$ the position of the center of mass
- $v_{\rm g} = \dot{x}_{\rm g} \in \boldsymbol{R}^3$ the velocity of the center of mass
- $R \in SO^+(3)$ the orientation of the body-fixed frame with respect to a given inertial frame
- $\Omega \in \boldsymbol{R}^3$ the angular velocity of the body expressed in the body–fixed frame.

Relation between Ω and R

$$\widetilde{\Omega} = R^\top \dot{R}, \tag{7}$$

or equivalently,

$$\dot{R} = R\widetilde{\Omega}, \qquad \text{(Lie-type ODE)} \tag{8}$$

where the matrix $\widetilde{\Omega} \in \boldsymbol{R}^{3\times 3}$ is given by $\widetilde{\Omega}x = \Omega \times x$ for all $x \in \boldsymbol{R}^3$.

Newton-Euler formulation of the equation of motion

Newton–Euler equations of motion

$$\begin{cases} m\,\dot{v}_{\rm g} &= f(t, x_{\rm g}, v_{\rm g}, R, \Omega) \\ I\dot{\Omega} + \Omega \times I\Omega &= M(t, x_{\rm g}, v_{\rm g}, R, \Omega) \\ \dot{x}_{\rm g} &= v_{\rm g} \\ \dot{R} &= R\widetilde{\Omega} \end{cases} \tag{9}$$

where

- $m > 0$ is the mass,
- $I \in \boldsymbol{R}^{3\times 3}$ is the matrix of moments of inertia around the center of mass and the axis of the body–fixed frame
- $f(\cdot) \in \boldsymbol{R}^3$ and $M(\cdot) \in \boldsymbol{R}^3$ are the total forces and torques applied to the body.

Possible rotation parameterization

Matrix parametrization $R \in SO(3)$

It introduces numerous redundant parameters that are solved by

$$\det(R) = 1 \quad \text{and} \quad R^{-1} = R^\top$$

Unit quaternion parametrization $p \in \boldsymbol{H}_1$

Quaternion parametrization $p \in \boldsymbol{H}$ (isomorphic to $\boldsymbol{R}^4$) with only one redundant parameter solved by

$$\|p\| = 1$$

Representation in $\boldsymbol{R}^4$: $p = (p_0, p_1, p_2, p_3)$ $\|p\|^2 = p_o^2 + p_1^2 + p_2^2 + p_3^2$
Representation in $\boldsymbol{R} \times \boldsymbol{R}^3$ $p = (p_0, \vec{p})$
Quaternion product.

$$p \cdot q = \begin{bmatrix} p_o q_o - \vec{p}\,\vec{q} \\ p_0 \vec{q} + q_o \vec{p} + \vec{p} \times \vec{q} \end{bmatrix}. \tag{10}$$

Adjoint quaternion

$$p^\star = (p_0, -\vec{p}) \tag{11}$$

Possible rotation parameterization

Unit quaternion parametrization $p \in \boldsymbol{H}_1$

For two vectors $x \in \boldsymbol{R}^3$ and $x' \in \boldsymbol{R}^3$, we define the quaternion $p_x = (0, x) \in \boldsymbol{H}_p$ and $p_{x'} = (0, x') \in \boldsymbol{H}_p$. For a given unit quaternion p, the transformation

$$p_{x'} = p \cdot p_x \cdot p^\star \tag{12}$$

defines a rotation R such that $x' = Rx$ given by

$$x' = (p_0^2 - p^\top \vec{p})x + 2p_0(\vec{p} \times x) + 2(\vec{p}^\top x)p = Rx \tag{13}$$

The rotation matrix may be computed as

$$R = \Phi(p) = \begin{bmatrix} 1 - 2p_2^2 - 2p_3^2 & 2(p_1p_2 - p_3p_0) & 2(p_1p_3 + p_2p_0) \\ 2(p_1p_2 + p_3p_0) & 1 - 2p_1^2 - 2p_3^2 & 2(p_2p_3 - p_1p_0) \\ 2(p_1p_3 - p_2p_0) & 2(p_2p_3 + p_1p_0) & 1 - 2p_1^2 - 2p_2^2 \end{bmatrix} \tag{14}$$

Possible rotation parameterization

Compact form of the coordinates and the body twist

We denote by q the vector of coordinates of the position and the orientation of the body, and by v the body twist:

$$q := \begin{bmatrix} x_{\mathrm{g}} \\ p \end{bmatrix}, \quad v := \begin{bmatrix} v_{\mathrm{g}} \\ \Omega \end{bmatrix}. \tag{15}$$

Possible rotation parameterization

Lie type ode in terms of quaternion

Matrix rotation $\dot{R} = R\tilde{\Omega}$
The time derivative of $p_{x'} = p \cdot p_x \cdot p^\star$ yields

$$\dot{p}_{x'}(t) = \frac{1}{2} p(t) \cdot (0, \Omega(t)) = \cdot \hat{\Omega} \quad \text{(Lie-type ODE)} \tag{16}$$

where $\hat{x}$ is the unit quaternion associated with a vector $x \in \boldsymbol{R}^3$ such that $\hat{x} = (0, x)$
In matrix notation, we define $\dot{p} = \Psi(p)\Omega$, the relation between v and the time derivative of q is

$$\dot{q} = \begin{bmatrix} \dot{x}_{\text{g}} \\ \Psi(p)\dot{p} \end{bmatrix} = \begin{bmatrix} I & 0 \\ 0 & \Psi(p) \end{bmatrix} v := T(q)v \tag{17}$$

with $T(q) \in \boldsymbol{R}^{7\times 6}$.

Compact form of the Newton-Euler equation

$$\begin{cases} \dot{q} = T(q)v, \\ M\dot{v} = F(t, q, v) \end{cases} \tag{18}$$

where $M \in \mathbb{R}^{6\times 6}$ is the total inertia matrix

$$M := \begin{pmatrix} mI_{3\times 3} & 0 \\ 0 & I \end{pmatrix}, \tag{19}$$

and $F(t, q, v) \in \mathbb{R}^6$ collects all the forces and torques applied to the body

$$F(t, q, v) := \begin{pmatrix} f(t, x_{\mathrm{g}}, v_{\mathrm{g}}, R, \Omega) \\ I\Omega \times \Omega + M(t, x_{\mathrm{g}}, v_{\mathrm{g}}, R, \Omega) \end{pmatrix}. \tag{20}$$

Joints and unilateral constraints

Bilateral constraints

- Coordinate level

$$h^\alpha(q) = 0, \alpha \in \mathcal{E} \subset \mathbf{N}, |\mathcal{E}| = m_e, \tag{21}$$

- Body twist level
  $J_h^\alpha(q) = \nabla_q^\top h^\alpha(q)$ the Jacobian matrix of $h^\alpha(q)$ with respect to q.
  The bilateral constraints at the velocity level can be obtained as:

$$0 = \dot{h}^\alpha(q) = J_h^\alpha(q)\dot{q} = J_h^\alpha(q)T(q)v := H^\alpha(q)v, \quad \alpha \in \mathcal{E}. \tag{22}$$

associated with a Lagrange multiplier $\lambda^\alpha, \alpha \in \mathcal{E}$ that generates a force applied to the body

$$H^{\alpha,\top}(q)\lambda^\alpha. \tag{23}$$

Joints and unilateral constraints

Bilateral constraints

- Coordinate level

$$g_{\mathrm{N}}^{\alpha}(q) \geqslant 0, \alpha \in \mathcal{I} \subset \boldsymbol{N}, |\mathcal{I}| = m_i. \tag{24}$$

- Body twist level
  $J_{g_{\mathrm{N}}}^{\alpha}(q)$ respectively for $g_{\mathrm{N}}^{\alpha}(q)$ the Jacobian matrix of $g_{\mathrm{N}}^{\alpha}(q)$ with respect to q.

$$0 \leqslant \dot{g}_{\mathrm{N}}^{\alpha}(q) = J_{g_{\mathrm{N}}}^{\alpha}(q)\dot{q} = J_{g_{\mathrm{N}}}^{\alpha}(q)T(q)v, \text{ if } g_{\mathrm{N}}^{\alpha}(q) = 0, \quad \alpha \in \mathcal{I}. \tag{25}$$

Remark

There is no reason that $\lambda_{\mathrm{N}}^{\alpha} = r_{\mathrm{N}}^{\alpha}$ and $u_{\mathrm{N}}^{\alpha} = J_{g_{\mathrm{N}}}^{\alpha}(q)T(q)v$ if the function g_n is not chosen as the signed distance (the gap function)

Joints and unilateral constraints

Unilateral constraints

Body twist level in terms of unknowns in the local frame

$$u_{\mathrm{N}}^{\alpha} := G_{\mathrm{N}}^{\alpha}(q)v, \quad u_{\mathrm{T}}^{\alpha} := G_{\mathrm{T}}^{\alpha}(q)v, \quad \alpha \in \mathcal{I}, \tag{26}$$

or more compactly

$$u^{\alpha} := G^{\alpha}(q)v \tag{27}$$

associated with the total force generated by the contact α as

$$G^{\alpha,\top}(q)r^{\alpha} := G_{\mathrm{N}}^{\alpha,\top}(q)r_{\mathrm{N}}^{\alpha} + G_{\mathrm{T}}^{\alpha,\top}(q)r_{\mathrm{T}}^{\alpha} \tag{28}$$

Newton-Euler equations with constraints

Newton–Euler equations

$$\left\{\begin{array}{lll} \dot{q} = T(q)v, & & \\ M\dot{v} = F(t,q,v) + H^\top(q)\lambda + G^\top(q)r, & & \\ H^\alpha(q)v = 0, \quad \lambda^\alpha & & \alpha \in \mathcal{E} \\ \left.\begin{array}{ll} r^\alpha = 0, & \text{if } g_N^\alpha(q) > 0, \\ K^{\alpha,*} \ni \widehat{u}^\alpha \perp r^\alpha \in K^\alpha, & \text{if } g_N^\alpha(q) = 0, \\ u_N^{\alpha,+} = -e_r^\alpha u_N^{\alpha,-}, & \text{if } g_N^\alpha(q) = 0 \text{ and } u_N^{\alpha,-} \leqslant 0 \end{array}\right\} & & \alpha \in \mathcal{I}, \end{array}\right. \tag{29}$$

Index-2 stabilized formulation

Application of the Gear–Gupta–Leimkuhler (GGL) method to stabilize the constraints at the coordinate level:

$$
\left\{
\begin{array}{ll}
\dot{q} = T(q)v + J_h^\top(q)\mu + J_{g_\mathrm{N}}^\top(q)\tau, & \\
M\dot{v} = F(t,q,v) + H^\top(q)\lambda + G^\top(q)r, & \\
\quad \left.\begin{array}{ll} H^\alpha(q)v = 0, \quad \lambda^\alpha & \\ h^\alpha(q) = 0, \quad \mu^\alpha & \end{array}\right\} & \alpha \in \mathcal{E} \\
\quad \left.\begin{array}{ll} r^\alpha = 0, & \text{if } g_\mathrm{N}^\alpha(q) > 0, \\ K^{\alpha,*} \ni \widehat{u}^\alpha \perp r^\alpha \in K^\alpha, & \text{if } g_\mathrm{N}^\alpha(q) = 0, \\ u_\mathrm{N}^{\alpha,+} = -e_r^\alpha u_\mathrm{N}^{\alpha,-}, & \text{if } g_\mathrm{N}^\alpha(q) = 0 \text{ and } u_\mathrm{N}^{\alpha,-} \leqslant 0, \\ 0 \leqslant g_\mathrm{N}(q) \perp \tau \geqslant 0 & \end{array}\right\} & \alpha \in \mathcal{I}.
\end{array}
\right.
\tag{30}
$$

In a continuous time setting, we can show that the multipliers μ and τ vanish.

Principles of the Moreau–Jean scheme

- Reformulation of the dynamics in terms of differential measure.
- Second order sweeping process that includes the complementarity at the velocity level with the Newton-impact law
- Main unknowns are the velocities and the impulses.

Principles of the Moreau–Jean scheme

Dynamics in terms of measures

$$\left\{ \begin{array}{l} \dot{q} = T(q)v + J_h^\top(q)\mu + J_{g_\mathrm{N}}^\top(q)\tau, \\ M\mathrm{d}v = F(t,q,v)\mathrm{d}t + H^\top(q)\mathrm{d}i_\lambda + G^\top(q)\mathrm{d}i_r, \end{array} \right.$$

Second order sweeping process

$$\left. \begin{array}{lr} \mathrm{d}i_r^\alpha = 0, & \text{if } g_\mathrm{N}^\alpha(q) > 0, \\ K^{\alpha,*} \ni \widehat{u}^{\alpha,+} + e_r^\alpha u_\mathrm{N}^{\alpha,-}\mathrm{N} \quad \perp \mathrm{d}i_r^\alpha \in K^\alpha, & \text{if } g_\mathrm{N}^\alpha(q) = 0, \end{array} \right\} \qquad \alpha \in \mathcal{I}. \tag{31}$$

Principles of the Moreau–Jean scheme

Main unknowns are the velocities and the impulses.

Integration over a time-interval $(t_k, t_{k+1}]$:

$$\int_{(t_k,t_{k+1}]} M\mathrm{d}v = M(v^+(t_{k+1}) - v^+(t_k)) \approx M(v_{k+1} - v_k) \tag{32}$$

➜v_k is a approximation of $v^+(t_k)$

$$\int_{(t_k,t_{k+1}]} \mathrm{d}i_\lambda \approx Q_{k+1} \qquad \int_{(t_k,t_{k+1}]} \mathrm{d}i_r \approx P_{k+1} \tag{33}$$

➜Q_{k+1} and P_{k+1} are direct approximations of the impulses over the time interval

$$\int_{t_k}^{t_{k+1}} J_h^\top(q)\mu(t)\mathrm{d}t \approx \gamma_{k+1}, \quad \int_{t_k}^{t_{k+1}} J_{g_\mathrm{N}}^\top(q)\tau(t)\mathrm{d}t \approx \delta_{k+1}, \tag{34}$$

Numerical integration scheme

Standard activation rule

$$\mathcal{I}_k = \{\alpha \in I \mid g^\alpha_{\mathrm{N},k} + \gamma u^\alpha_{\mathrm{N},k} \leqslant 0\} \text{ with } \gamma \in [0, \frac{1}{2}] \tag{35}$$

Direct GGL approach

$$\begin{cases} q_{k+1} = q_k + hT(q_{k+\theta})v_{k+\theta} + J_h^\top(q_{k+1})\gamma_{k+1} + J_{g_\mathrm{N}}^\top(q_{k+1})\delta_{k+1}, \\ M(v_{k+1} - v_k) - hF_{k+\theta} = H^\top(q_{k+1})Q_{k+1} + G^\top(q_{k+1})P_{k+1}, \\ \left.\begin{array}{l} H^\alpha(q_{k+1})v_{k+1} = 0 \\ h^\alpha(q_{k+1}) = 0 \end{array}\right\} \quad \alpha \in \mathcal{E} \\ \left. P^\alpha_{k+1} = 0, \delta^\alpha_{k+1} = 0, \right\} \quad \alpha \notin \mathcal{I}_k \\ \left.\begin{array}{l} K^{\alpha,*} \ni \widehat{u}^\alpha_{k+1} + e^\alpha_r u^\alpha_{\mathrm{N},k}\mathrm{N} \perp P^\alpha_{k+1} \in K^\alpha \\ g^\alpha_{\mathrm{N},k+1} = 0, \delta^\alpha_{k+1}, \text{ if } P^\alpha_{\mathrm{N},k+1} > 0, \\ 0 \leqslant g^\alpha_{\mathrm{N},k+1} \perp \delta^\alpha_{k+1} \geqslant 0 \text{ otherwise} \end{array}\right\} \quad \alpha \in \mathcal{I}_k. \end{cases} \tag{36}$$

The notation $x_{k+\theta} = (1-\theta)x_k + \theta x_{k+1}$ is used for $\theta \in [0, 1]$.

Numerical integration scheme

The direct GGL approach yields spurious oscillations when a contact is closing.

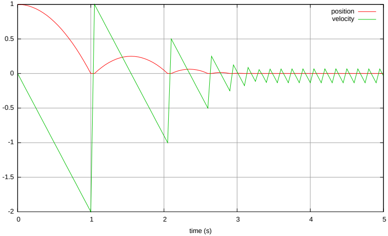

(a) Approximate position and velocity for $\gamma = 0$

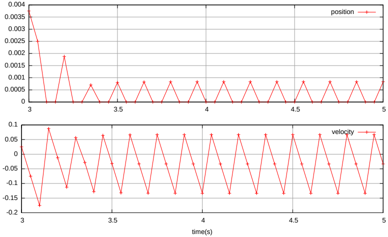

(b) Zoom on $t \in [3, 5]$for $\gamma = 0$

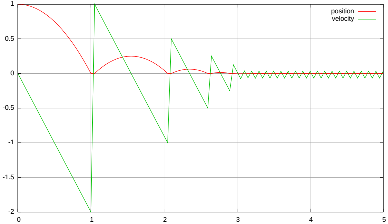

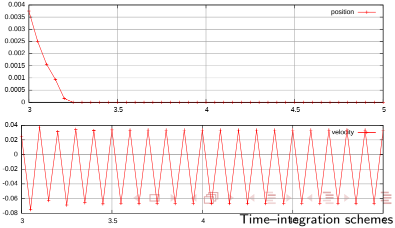

Numerical integration scheme

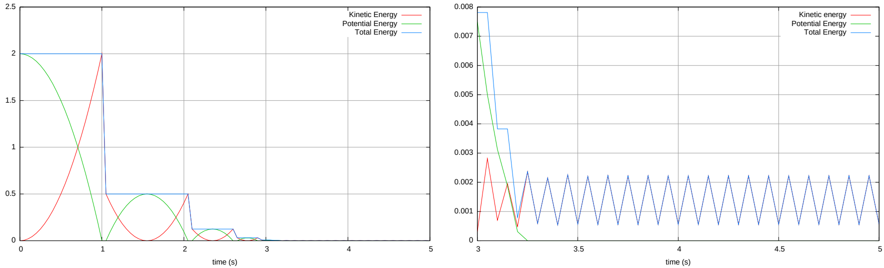

(a) Energy diagram $\theta = 1/2$. $\gamma = 1$

(b) Zoom on $t \in [3, 5]$ Energy diagram $\theta = 1/2$. $\gamma = 1$

Figure: Energy for the bouncing ball). $h = 5.10^{-2}$

Numerical integration scheme

Energy Balance in Elastic case

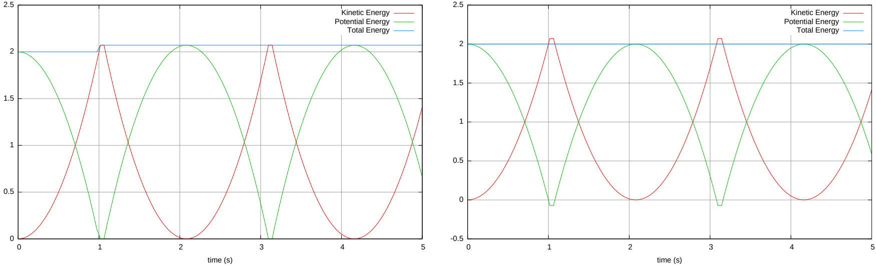

(a) Energy diagram $\theta = 1/2$ with projection

(b) Energy diagram $\theta = 1/2$ without projection

Figure: Energy in the elastic case ($e = 1$) for the bouncing ball. $h = 5.10^{-2}$

Numerical integration scheme

A combined scheme with a projection step and an activation step

Projection step for a given index set of active constraints $\mathcal{I}^\nu$.

$$\left\{\begin{array}{ll}
q_{k+1} = q_k + hT(q_{k+\theta})v_{k+\theta} + J_h^\top(q_{k+1})\gamma_{k+1} + J_{g_\mathrm{N}}^\top(q_{k+1})\delta_{k+1}, & \\
M(v_{k+1}-v_k) - hF_{k+\theta} = H^\top(q_{k+1})Q_{k+1} + G^\top(q_{k+1})P_{k+1}, & \\
\left.\begin{array}{l} H^\alpha(q_{k+1})v_{k+1} = 0 \\ h^\alpha(q_{k+1}) = 0 \end{array}\right\} & \alpha \in \mathcal{E} \\
\left.P^\alpha_{k+1} = 0, \delta^\alpha_{k+1} = 0,\right\} & \alpha \notin \mathcal{I}^\nu \\
\left.\begin{array}{l} K^{\alpha,*} \ni \widehat{u}^\alpha_{k+1} + e^\alpha_r u^\alpha_{\mathrm{N},k}\mathrm{N} \perp P^\alpha_{k+1} \in K^\alpha \\ g^\alpha_{\mathrm{N},k+1} = 0, \delta^\alpha_{k+1}, \text{ if } P^\alpha_{\mathrm{N},k+1} > 0, \\ 0 \leqslant g^\alpha_{\mathrm{N},k+1} \perp \delta^\alpha_{k+1} \geqslant 0 \text{ otherwise} \end{array}\right\} & \alpha \in \mathcal{I}^\nu.
\end{array}\right. \quad (37)$$

➜ we obtain an estimation of the gap at step ν : $g^\nu_{\mathrm{N},k+1}$

Numerical integration scheme

A combined scheme with a projection step and an activation step

Activation step:

- $\mathcal{I}^0 = \emptyset$
- Update of the active set of constraints:

$$\mathcal{I}^{\nu+1} = \mathcal{I}^{\nu} \cup \left\{\alpha \in \mathcal{I} \mid g^{\alpha,\nu}_{\mathrm{N},k+1} \leqslant 0\right\}. \tag{38}$$

Numerical integration scheme

Unit quaternion drift off effect

The integration rule of $\dot{q} = T(q)v$ as

$$q_{k+1} = q_k + hT(q_{k+\theta})v_{k+\theta} \tag{39}$$

or most precisely, for $\dot{p} = \Psi(p)\Omega$ as

$$p_{k+1} = p_k + h\Psi(q_{k+\theta})\Omega_{k+\theta} \tag{40}$$

does not conserve the unit quaternion constraints.
A possible choice is to project onto the unit quaternion set $\boldsymbol{H}_1$

Numerical integration scheme

Lie group integration scheme

The Lie ordinary differential equation

$$\dot{p}(t) = \Psi(p(t))\Omega = p(t) \cdot \hat{\Omega}, \quad p(0) = p_0 \tag{41}$$

has an exact integration rule in $\boldsymbol{H}_1$ given by

$$p(t) = p_0 \operatorname{expq}(t\hat{\Omega}) \tag{42}$$

where expq is the exponential of a quaternion

$$\operatorname{expq}(\widehat{\Omega}) = (\cos(\frac{\theta}{2}), \sin(\frac{\theta}{2})\frac{\Omega}{\theta}). \tag{43}$$

Numerical integration scheme

Lie group integration scheme

Similarly [Simo and Wong, 1991, Brüls and Cardona, 2010], we proposed the following integration rule

$$p_{k+1} = p_k \operatorname{expq}(h\hat{\Omega}_{k+\theta}) \tag{44}$$

that ensures the conservation of the constraints $\|p_{k+1}\| = 1$.

A further question is to extend this rule to the GGL approach.

Application to a mechanism of a circuit breaker

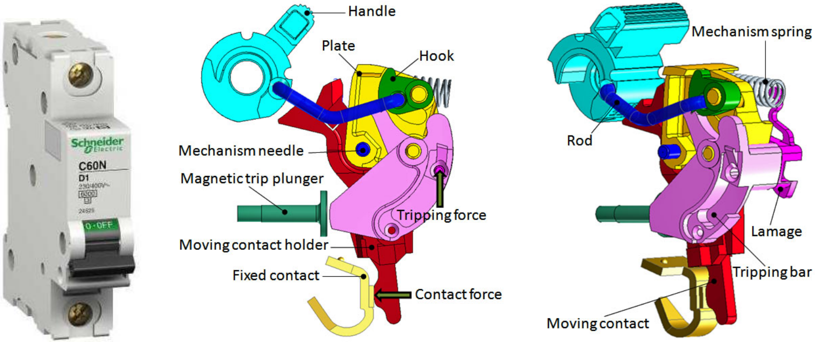

(a) External view (b) View-1. (c) View-2.

Figure: Schneider Electric C-60 circuit breaker mechanism.

Application to a mechanism of a circuit breaker

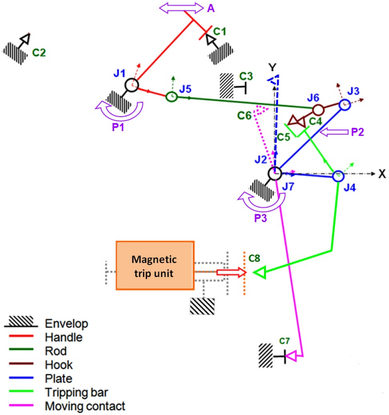

(a) ON (close) position.

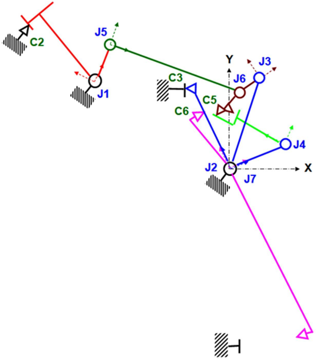

(b) OFF (trip or open) position.

Figure: Kinematic representations of the C-60 mechanism.

Application to a mechanism of a circuit breaker

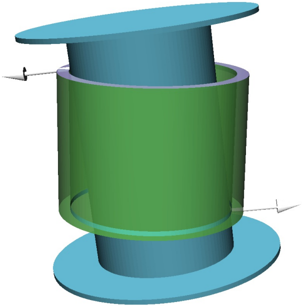

(a) Cylinder/Cylinder contact with axial mis-alignment

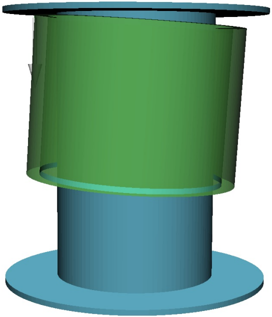

(b) Cylinder/plane contact for contact with flanges.

Figure: Two kinds of contacts in spatial revolute joint with clearances showing contact forces in siconos.

Application to a mechanism of a circuit breaker

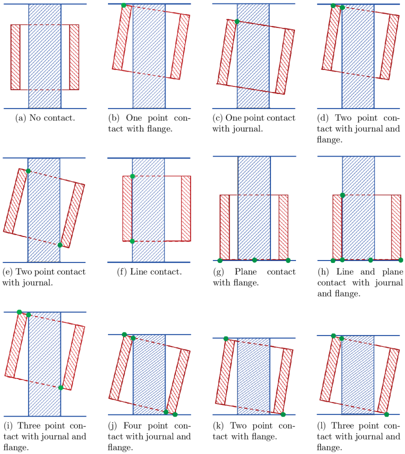

Figure: Two kinds of contacts in spatial revolute joints with clearances

Application to a mechanism of a circuit breaker

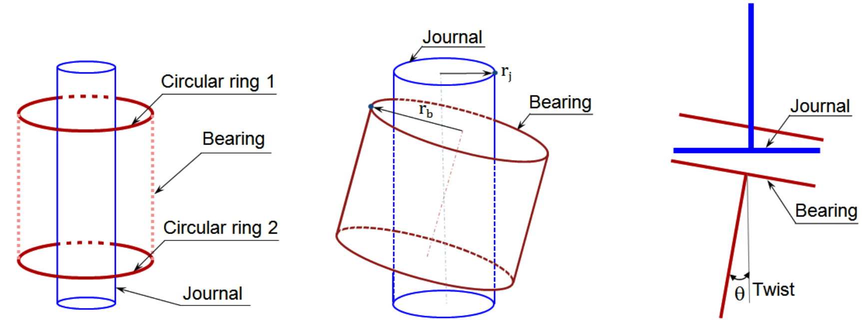

(a) Gap distance are computed between the circular rings (in red) and the journal cylinder (in blue)

(b) Axial mis-alignment

(c) Polarization effect: out-of-plane motion of the mechanism due to clearances.

Figure: Generic representation of a 3D revolute joint with clearance : cylinder/cylinder contact

Application to a mechanism of a circuit breaker

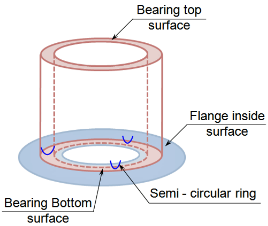

Figure: Modelling of plane–plane contact between the bearing and the journal flanges or plane stops.

Application to a mechanism of a circuit breaker

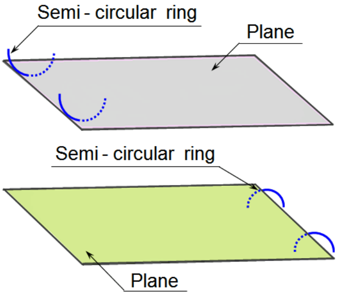

(a) Plane surface and two semi-circular rings for the first plane surface.

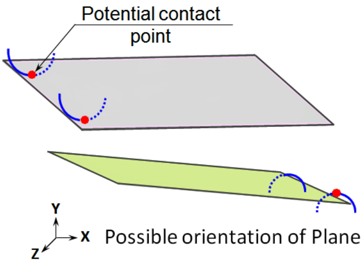

(b) Plane surface and two semi-circular rings for the second plane surface.

Figure: Strategy to model the plane-plane contact.

Application to a mechanism of a circuit breaker

Software

- Siconos is used for the time integration and for solving the discrete frictional contact problem
- OpenCascade and PythonOCC are used for the CAD modeling and the computation of contact distance and local frame at contact

Experimental validation

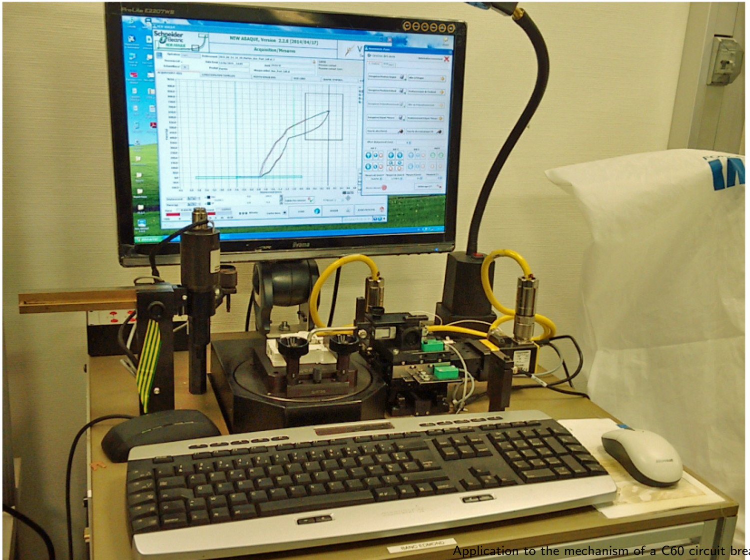

Experimental validation

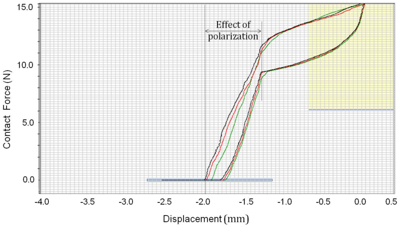

(a) Experimental result.

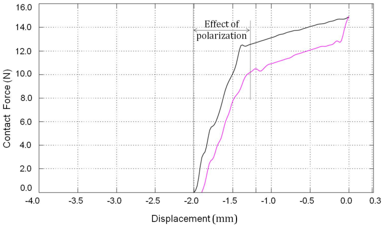

(b) Simulation result.

Figure: Contact force versus displacement.

Experimental validation

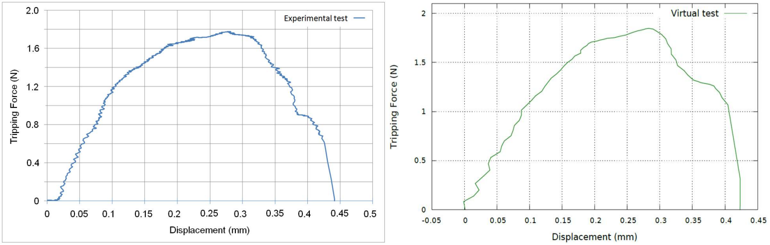

(a) Experimental test (b) Virtual (numerical) test

Figure: Tripping force vs displacement: pin-side.

Sensitivity Analysis

Functional conditions

Table: Output variables of the C-60 breaker.

FC - Name	Description of the Functional Conditions (FC)
FC - 1	Contact Force (N)
FC - 2	Distance between Needle - Tripping bar pin position in X direction (mm)
FC - 3	Distance between Needle - Tripping bar pin position in Y direction (mm)
FC - 4	Distance between Needle - Lamage in X direction (mm)
FC - 5	Distance between Needle - Lamage in Y direction (mm)
FC - 6	Distance between Tripping bar - Plunger in X direction (mm)

Sensitivity Analysis

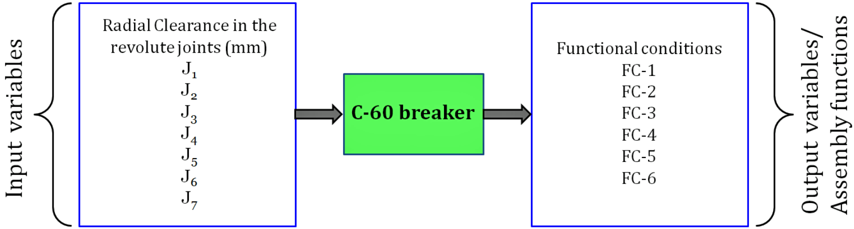

Figure: Variables in the statistical analysis.

Sensitivity Analysis

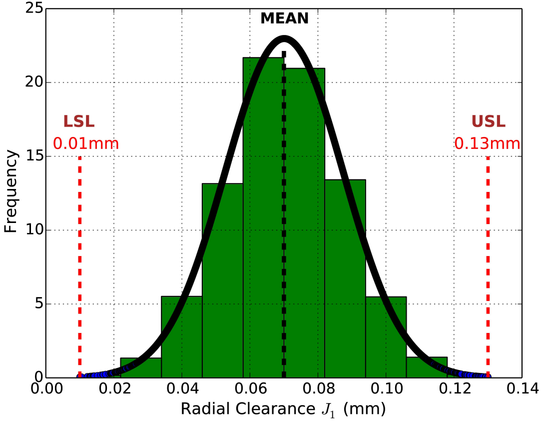

(a) Joints $J_1, \ldots, J_7$, $\bar{m} = 0.07\,\mathrm{mm}$, $\sigma = 0.0175$.

Figure: Generated random numbers for the joints J_1, J_2, J_3, J_4, J_5, J_6 and J_7.

Sensitivity Analysis

Key numbers

- 30 850 simulations
- Avg. simulation time per simulation 810 s

Sensitivity Analysis

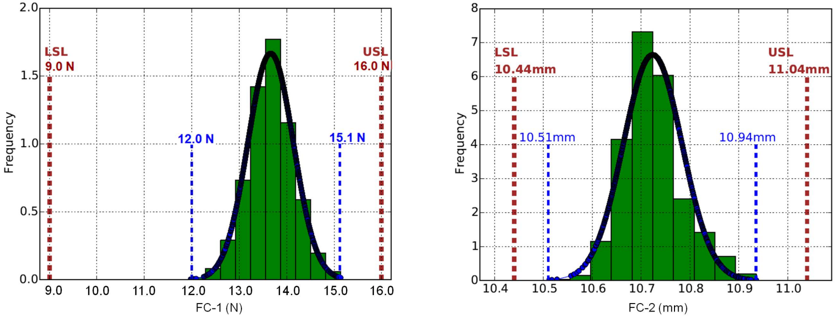

(a) FC-1, $\bar{m} = 13.66\,\mathrm{N}$, $\sigma = 0.239$.

(b) FC-2, $\bar{m} = 10.724\,\mathrm{mm}$, $\sigma = 0.060$.

Figure: Dispersion of the functional conditions: FC-1 and FC-2.

Thank you for your attention.

O. Brüls and A. Cardona. On the use of Lie group time integrators in multibody dynamics. *ASME Journal of Computational and Nonlinear Dynamics*, 5(031002), 2010.

J.C. Simo and K. Wong. Unconditionnally stable algorithms for rigid body dynamics that exactly preserve energy and momentum. *International Journal for Numerical Methods in Engineering*, 31:19–52, 1991.